https://dx.doi.org/10.21577/0103-5053.20210071

J. Braz. Chem. Soc., Vol. 32, No. 9, 1802-1812, 2021

Article

Synthesis, Structure Determination and Catalytic Activity of a Novel Ruthenium(II) [RuCl(dppb)(44bipy)(4-pic)]PF_6 Complex

Rafael G. da Silveira, *,[a,b] *Angel R. Higuera-Padilla,*[a,c] *Beatriz N. da Cunha,*[a,b] *João H. de Araujo Neto,*[a] *Anderson J. L. Catão,*[a] *Luiz A. Colnago,*[c] *Eduardo E. Castellano*[d] *and Alzir A. Batista* *,[a]

[a]*Departamento de Química, Universidade Federal de São Carlos (UFSCar), 13560-970 São Carlos-SP, Brazil*

[b]*Departamento de Química, Instituto Federal Goiano, Campus Ceres, 76300-000 Ceres-GO, Brazil*

[c]*Laboratório de Ressonância Magnética Nuclear, Embrapa Instrumentação, 13560-970 São Carlos-SP, Brazil*

[d]*Instituto de Física de São Carlos, Universidade de São Paulo, CP 369, 13560-970 São Carlos-SP, Brazil*

This work reports the synthesis, structure and catalytic activity of a novel ruthenium(II) complex, [RuCl(dppb)(44bipy)(4-pic)]PF_6 (where dppb = 1,4-bis(diphenylphosphine)butane; 44bipy = 4,4'-dimethyl-2,2'-dipyridyl; 4-pic = 4-picoline). The molecular structure and catalytic activity were studied by Fourier transform infrared (FTIR), UV-Vis and nuclear magnetic resonance (NMR) spectroscopies, cyclic voltammetry, and X-ray crystallography, while the electronic structure was investigated by density-functional theory (DFT) and time dependent DFT (TD-DFT) methods. Electrochemical studies showed the substitution of the chlorido ligand from the precursor by the 4-pic ligand, exhibiting the Ru^{II}/Ru^{III} process at 1.21 V. The structure of the compound was optimized using DFT simulations and showed data similar to the X-ray structure. The UV-Vis absorption spectrum showed a good agreement with TD-DFT simulations. The highest occupied molecular orbital (HOMO) and the lowest unoccupied molecular orbital (LUMO) energies were determined at the Becke, 3-parameter, Lee-Yang-Parr (B3LYP) level. The study of the catalytic activity in the transfer hydrogenation of ketones by the ^{1}H NMR showed efficient transfer hydrogenation reaction at 60 ºC, employing acetophenone as substrate and resulting in a high conversion. The formation of two ruthenium-hydride species was observed.

Keywords: ruthenium complex, DFT calculations, hydrogenation transfer catalysis, NMR monitoring

Introduction

Several research groups on reactions catalyzed by transition metal compounds have been dedicated to the study of new compounds due to various academic and industrial applications. Reactions of transfer hydrogenation by alcohols as the hydrogen source catalyzed by metal complex have been widely reported as an effective protocol, and in this area, ruthenium catalysts stand out.[1-4] Geoffrey Wilkinson and co-workers[5] studied these compounds that show enhanced stability, good selectivity and high catalytic activity. They examined the proprieties of ruthenium/rhodium/phosphine complexes in catalytic hydrofunctionalization reactions such as hydroacylation, hydroboration and hydrosilylation of alkenes.[2,3,5] Moreover, many studies have investigated the proprieties of Wilkinson's catalyst and analogues, resulting in a wide range of applications of these complexes such as anticancer and antibacterial drugs.[6-8]

The hydrogenation of ketones to alcohols using isopropanol as a hydrogen source has attracted wide attention because isopropanol is a common and cheap solvent; isopropanol and the by-product of the hydrogenation transfer reaction, acetone, are volatile which

*e-mail: rafael.silveira@ifgoiano.edu.br; daab@ufscar.br

simplify the purification of the product; the reaction does not need pressurized hydrogen gas, nor does it produce hazardous waste. This hydrogenation transfer reaction can be performed in basic medium. Therefore, developing substances with catalytic proprieties under neutral conditions is highly recommended, mainly utilizing more sustainable and economic catalytic systems for this kind of hydrogenation reaction.[9-12]

In previous works,[13-15] our research group reported on the catalytic profile of some complexes of [Ru(P-P)(N-N)L] type (P-P = biphosphine; N-N = bipyridine and L = mono/bidentade ligand), showing that the ruthenium(II) complexes perform well as precursors in the hydrogenation of non-polar double bonds, transfer hydrogenation of polar double bonds, hydroformylation/hydrogenation, hydroformylation/acetalization and oxidation of alkenes.[13] Among these works, Rodrigues *et al.*[14] demonstrate that Ru^{II}/Ru^{III} complexes tested as hydroformylation-hydrogenation catalysts can produce up to 92% (isolated yield) of ethanol cyclohexane, without using additives, showing high versatility as a catalytic agent.[14] Another highlight is a study carried out by Higuera-Padilla *et al.*[15] which determines the complex catalytic mechanism of hydrogenation of ketones to alcohols with isopropanol as a hydrogen source, monitoring the reaction *in situ* by rapid injection and in real time using ^{1}H nuclear magnetic resonance (NMR) spectroscopy techniques.[15] This shows that the reaction mechanism involves the formation of a hydride species and ketone followed by the reduction of ketone substrates, answering the main question of catalysis, the chemical reactions involved in the catalytic process.

In this study, we report on the synthesis, full characterization and theoretical calculations of a new ruthenium(II) complex with 4-picoline ligand. The structure of the complex was determined in crystalline state by X-ray crystallography. The structural analysis and characterization of the complex, in solution, were performed by NMR techniques (^{1}H, ^{13}C{^{1}H}, ^{1}H-^{1}H correlated spectroscopy (COSY), ^{1}H-^{13}C heteronuclear multiple bond coherence (HMBC) and ^{1}H-^{13}C heteronuclear single quantum coherence spectroscopy (HSQC)), infrared, UV-Vis spectroscopies, conductivity, cyclic voltammetry, elemental analysis and density-functional theory (DFT) calculations. Herein the catalytic activity of this complex is described, in a hydrogen transfer reaction from isopropanol to ketones. Different reaction conditions were used, which include different organic substrates, to produce alcohols. *In situ* high-field NMR spectroscopy was used to monitor the hydrogen transfer reaction in real-time with rapid injection NMR spectroscopy, which is a reliable tool for structural analysis and determination of reaction rates and yields.

Experimental

Materials for synthesis

Solvents used for the spectroscopic studies were of spectroscopic grade and were purified by standard methods. All chemicals used were of reagent grade or comparable purity. $RuCl_3 \cdot 3H_2O$ and ligands 1,4-bis(diphenylphosphino) butane (dppb) and 4,4'-dimethyl-2,2'-dipyridyl (44bipy), 4-methylpyridine (4-pic) were used as received from Sigma-Aldrich (St. Louis, USA). The precursor *cis*-[$RuCl_2$(dppb)(44bipy)] was prepared following the protocol described by Queiroz *et al.*[16]

Instrumentation

Elemental analyses were performed in a Fisons EA 1108 model (Thermo Scientific, Waltham, USA). The IR spectrum was recorded on a FT-IR Bomem-Michelson 102 spectrometer (Vancouver, Canada) in the 4000-400 cm^{-1} region using solid samples pressed in KBr pellets. UV-Vis spectra were recorded in a HP8452A (diode array) spectrophotometer (Avondale, USA). All solvents and reagents employed in this work presented analytical grade and were purchased from Sigma-Aldrich Brazil (São Paulo, Brazil). Solutions with the concentrations of 1.0×10^{-4} mol L^{-1} in dimethyl sulfoxide (DMSO) and quartz cells of 1.0 cm path length were used in the analysis. The electrochemical measurements (cyclic voltammetry) were performed in an electrochemical analyzer, BAS model 100B/W MF-9063 Bioanalytical Systems Instrument (West Lafayette, USA). The measurements were performed in dichloromethane solution (degassed with argon) at room temperature with tetrabutylammonium perchlorate (TBAP) as supporting electrolyte. The electrodes used (working and auxiliary) were platinum and Ag/AgCl as the reference electrode and the ferrocene in this system is oxidized at 0.43 V (Fc^+/Fc). The ^{1}H, distortionless enhancement by polarization transfer (DEPT)-135 and advanced 2D NMR techniques such as gradient enhanced, ^{1}H-^{1}H COSY and ^{1}H-^{13}C correlation HSQC were used. These analyses were performed in acetone-d_6 as a solvent in a 5 mm sample tube at 293 K in Bruker Ascend 600 MHz equipment (Ettlingen, DE). For ^{1}H and ^{13}C NMR resonances, splitting was reported as s = singlet, d = dublet, t = triplet and m = multiplet.

Synthesis of [RuCl(dppb)(44bipy)(4-pic)]PF_6

In a Schlenk flask 0.098 mmol (80 mg) of *cis*-[$RuCl_2$(dppb)(44bipy)] in 15 mL of methanol/dichloromethane (1:1 v/v), 0.098 mmol (9.2 mg) of 4-pic

was added. The solution was stirred for 20 min then 0.098 mmol of KPF_6 (18 mg) was added and allowed to react for 15 min. The reaction volume was reduced to ca. 1 mL and 10 mL of diethyl ether was added to yield an orange solid, which was filtered off, washed in water and diethyl ether, and dried under vacuum. The [RuCl(dppb)(44bipy)(4-pic)]PF_6 complex (C4B-4pic) was crystallized by slow evaporation of solvent (acetone/methanol, 1:1 v/v). The numbered structure for NMR assignment shown in Figure 1.

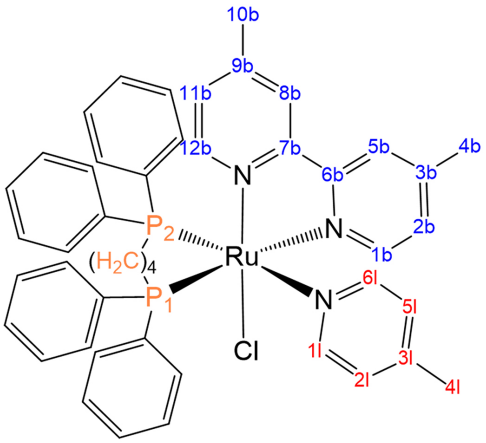

Figure 1. Structural representation of [RuCl(dppb)(44bipy)(4-pic)]PF_6 complex with numbered atoms for the NMR assignment.

[RuCl(dppb)(44bipy)(4-pic)]PF_6

Yield: 90%; orange solid; anal. calcd. for $C_{46}H_{47}ClF_6N_3P_3Ru$ C 56.07, H 4.81, N 4.26, found: C 56.19, H 4.94, N 4.28; UV-Vis (dichloromethane) λ / nm 290 (ε 16,317), 438 (ε 2,247); FTIR (KBr) ν / cm^{-1} 3056 ($C\text{-}H_{ar}$), 2915 and 2844 ($C\text{-}H_{sp^3}$), 1432 (C-N), 848 (P-F) + (P-C); $^{31}P\{^1H\}$ NMR (161.98 MHz, acetone-d_6, 298 K) δ 37.53 (d) and 37.26 (d) ($^2J_{P\text{-}P}$ 42.4 Hz); ^1H NMR (400.21 MHz, acetone-d_6, 298 K) δ 1.10-1.25 (m, 1H), 1.43-1.61 (m, 1H), 1.82-2.02 (m, 2H), 2.07 (s, 3H, 4l), 2.28-2.39 (m, 1H), 2.41 (s, 3H, 10b), 2.58 (s, 3H, 4b), 2.66-2.79 (m, 1H), 3.41-3.53 (m, 1H), 4.05-4.11 (m, 1H), 6.58 (d, 2H, *J* 5.7 Hz, (1l, 6l)), 6.86 (t, 2H, *J* 8.1 Hz), 6.95-7.01 (m, 3H, (11b, 2Ph)), 7.02-7.15 (m, 5H), 7.20-7.28 (m, 3H), 7.29-7.38 (m, 5H (2b, 4Ph)), 7.43 (m, 1H), 7.58 (m, 1H), 7.72 (t, 2H, *J* 8.0 Hz), 7.88-8.06 (m, 2H, (2l, 5l)), 8.16 (m, 1H, 8b), 8.35 (m, 1H, 5b), 8.89 (dd, *J* 5.8, 1.8 Hz, 12b), 9.07 (d, 1H, *J* 6.0 Hz, 1b); $^{13}C\{^1H\}$ NMR (100 MHz, acetone-d_6, 298 K) δ 20.31 (10b), 20.87 (4b), 21.56, 21.59, 24.43, 26.67, 26.98, 28.92, 30.10 (4l) 123.76 (8b), 125.63 (5b), 125.73 (1l, 6l), 128.34, 128.38, 128.41, 128.45, 128.84, 129.01, 129.09, 129.23, 129.30, 130.89, 131.73, 132.14, 132.20, 132.79, 132.86, 133.39, 133.48, 133.56, 133.71, 135.93, 136.28, 136.51, 136.59, 149.25 (3l), 150.41 (3b, 9b), 150.80 (12b), 151.03 (3l, 5l), 155.57 (7b), 158.63 (1b), 160.05 (6b).

X-ray crystallography

Single crystals of C4B-4pic were obtained by slow evaporation of solvent (acetone/methanol, 1:1 v/v) at room temperature. Single-crystals were selected and the intensity data were measured with the crystal at 293 K using the Enraf-Nonius Kappa-CCD diffractometer with graphite monochromated Mo Kα radiation (λ = 0.71073 Å) and the structures were solved by direct method using SHELXT. Non-hydrogen-atom positions were determined by Fourier-difference map analyses with refinements carried out with the SHELXL package using full-matrix least squares on F2 with anisotropic displacement parameters.[17] All H-atoms were stereochemically positioned and refined with the riding model. The visualization of the structure and tables with selected bond lengths and angles were generated using the Olex2[18] and Mercury[19] software.

Theoretical methods

Full geometry optimizations were performed from the crystallographic coordinates using the Becke's parameter hybrid functional combined with the Lee-Yang-Parr correlation functional (B3LYP) in Gaussian 09 package.[20] For ruthenium atoms, the Lanl2dz pseudopotential was used, while for light atoms, a full electron polarized double-zeta basis set 6-31G* was adopted.[21,22] Vibrational frequency analysis showed that optimized structure were real minima (no imaginary frequencies).[23-26] Time dependent DFT (TD-DFT) calculations were performed to obtain the UV-Vis analyzed using the Chemissian software in order to compare to experimental data.[27,28]

Monitoring the catalytic reaction by NMR spectroscopy

The study by NMR of the hydrogen transfer reaction from 2-propanol to one cyclic, one linear and one aromatic ketone, representing the different existing classes, was carried out in 5 mm NMR tubes in Bruker Ascend 600 MHz equipment. ^1H NMR spectra were acquired in deuterated benzene (C_6D_6), with sixteen scans, 30° pulse, acquisition time of 1.99 s and 1 s relaxation delay. Spectra were recorded at every 50 s, equivalent to approximately 600 spectra *per* reaction time. The reagents were added to NMR tubes, mixed and inserted into the spectrometer. After tube insertion in the probe, it was mandatory to allow a suitable time (10 min) to achieve thermal equilibrium. Sample temperature was established at 60 °C and controlled by the variable temperature heater of the probe. Following this, the catalyst precursor was injected through a cannula, coupled to a syringe and mechanically mixed by rapidly pushing and pulling, as was previously

reported.[15,29,30] Measurements began upon catalyst injection. The yield of the process was calculated by taking into account the relative integrals of ketone and alcohol.

Results and Discussion

The new monocationic [RuCl(dppb)(44bipy)(4-pic)]PF_6 complex was synthetized by the reaction of the precursor [$RuCl_2$(dppb)(44bipy)] in CH_2Cl_2/methanol (1:1, v/v) with the 4-methylpyridine ligand and the PF_6^- counter ion (orange solid). The synthesis scheme is presented in Figure 2.

The reaction was followed by $^{31}P\{^1H\}$ NMR, where the precursor consumption pathway can be followed, [$RuCl_2$(44bipy)(dppb)] in methanol/dichloromethane (1:1, v/v), which has two doublets spectrum, at 30.42 and 43.92 ppm, with *J* 39.2. After adding the 4-pic and KPF_6, we see the change in the spectrum to give two very close doublets with the appearance of a false singlet, as shown in Figure 3. This close proximity of the doublets shows that the two phosphorus atoms of the complex are in very similar chemical environments. This can be explained by the fact that one atom of phosphorus is *trans* to the N of the diiminic ligand, and the other atom of phosphorus is *trans* to the N of the 4-pic ligand.

The one-dimensional (1D) and two-dimensional (2D) ^1H and ^{13}C NMR experiments enabled the assignment the [Ru(dppb)(44bipy)(4-pic)Cl]PF_6 configuration. 1D ^1H and ^{13}C NMR, 2D ^{13}C-^1H HSQC, ^{13}C-^1H HMBC and ^1H-^1H-COSY in acetone-d_6 confirm the purity and the proposed structure and the assignment of the hydrogen and carbon atoms are shown in Figures S2-S6 (SI section). The ^1H spectrum is shown in Figure 4, where two major regions can be observed: an aliphatic region of 1.10-4.16 ppm totaling 17 H, attributed to 8 H from the $-CH_2-$ groups of the phosphine; and 9 H referring to the three methyl groups ($-CH_3$), consisting of 2 groups of the diiminic ligand and 1 of the 4-pic ligand. In the aromatic region of hydrogen, between 6.58-9.08 ppm with an integral of 30 H, there were 20 H of the 4 phenyl groups of the phosphine, 6 H of the diiminic ligand and 4 H of the 4-methylpyridine ligand. The experiment obtained for ^1H-^1H COSY identified the couplings between the more deshielded hydrogen 9.08 and 8.89 ppm which are attributed to the hydrogen neighboring the diimine nitrogen, which couples with the methyl groups of the diiminic ligand (2.56 and 2.39 ppm). In addition, the methyl group from the 4-pic ligand (2.07 ppm) couple to the hydrogens from the neighboring methyl groups from the 4,4'-bipyridine molecule. The hydrogens of the phenyl

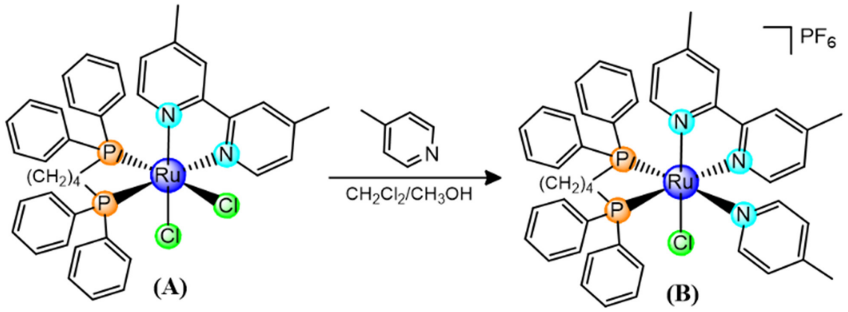

Figure 2. Route of synthesis for [RuCl(dppb)(44bipy)(4-pic)]PF_6 complex.

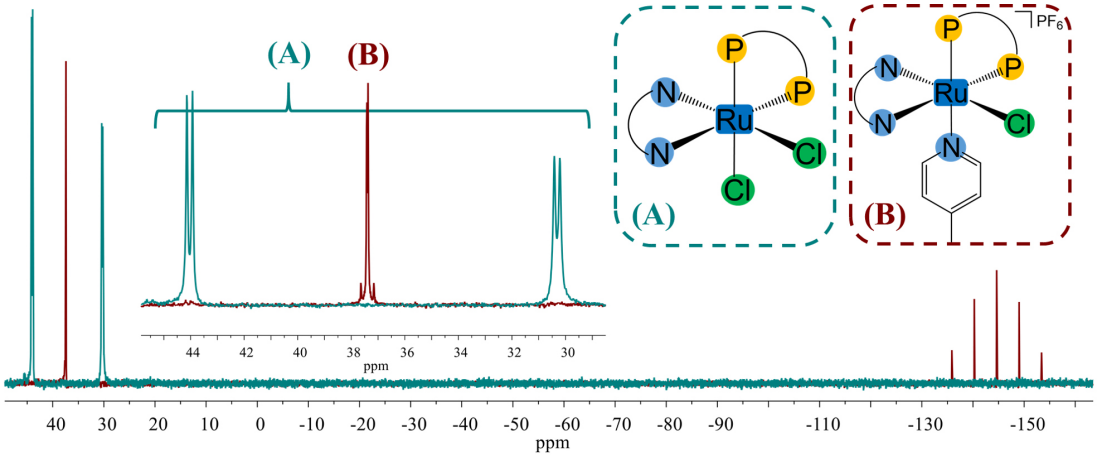

Figure 3. NMR spectrum $^{31}P\{^1H\}$ (161.98 MHz, CH_2Cl_2 with D_2O capillary) for A (precursor) and B for the [RuCl(dppb)(44bipy)(4-pic)]PF_6 complex.

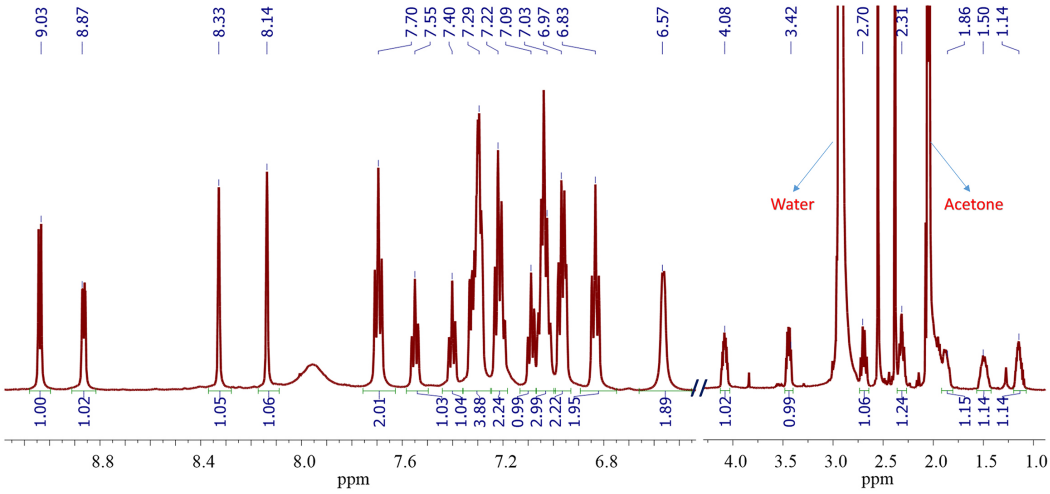

Figure 4. NMR ^{1}H spectrum (400.21 MHz, acetone-d_6) of the [RuCl(dppb)(44bipy)(4-pic)]PF_6 complex.

groups were not assigned to specific hydrogens because they are overlapped.

The $^{13}C\{^{1}H\}$ and DEPT-135 spectra are shown in Figure S3 (SI section) and the carbon type of each signal can be observed, $-CH_3-$, $-CH_2-$, $-CH-$ or $-C-$, which together with the data of ^{1}H-^{13}C HSQC can assign all the hydrogens of the diimine ligand and 4-pic. Carbon at 158.63 and at 150.80 ppm are attributed to hydrogens with signals at 9.08 and at 8.89 ppm, respectively. The carbons of the methyl groups of the diimine ligand are at 20.31 and at 20.87 ppm, bound to the hydrogens with chemical shifts at 2.40 and at 2.58 ppm and the carbon from the 4-pic ligand, in 30.10 ppm, is bound to the hydrogens with a chemical shift at 2.07 ppm.

The FTIR spectra of the precursor [$RuCl_2$(dppb)(44bipy)] and of the [RuCl(dppb)(44bipy)(4-pic)]PF_6 complex, shown in Figure S1 (SI section), are very similar to each other due to the chlorido ligand, because the ligand inserted in the complex does not present any characteristic functional group different from the precursor complex, resulting in few alterations in the profile of the bands presented in the FTIR spectra. When compared to the spectrum of the complex with that of the precursor, it is not possible to notice significant modifications in the spectrum because in the precursor there is already the stretching band νCH_{sp3} at 2848 and at 2922 cm^{-1} and at 3062 cm^{-1} referring to νCH_{arom} of the groups. Thus, the main evidence of the reaction is the appearance of the band at 845 cm^{-1} for the combination band νP–C and νP–F.

The precursor and the new complex were characterized by cyclic voltammetry (CV) experiments in 0.1 mol L^{-1} TBAP solution in dichloromethane, showing that both compounds are electroactive and the electrochemical behavior shows the change of the chemical environment in the coordination sphere of the metal, after the reaction. The behavior of the reaction can be followed by tracing the redox process in the precursor in approximately 0.76 V, which corresponds to the redox Ru^{II}/Ru^{III} process, while the product of the reaction shows the metal oxidation process at higher value, at 1.21 V, indicating the change in the coordination sphere of the metal, when a chlorido ligand is replaced by the 4-pic ligand. The voltammograms can be found in Figures S7 and S8 (SI section). In this reaction, the substitution of a donor sigma bond (Cl) ligand by a π-acceptor ligand (4-pic) can be seen removing the electronic density of the metal, which causes the displacement of the oxidation processor to the higher potential in the cyclic voltammogram. These data are in accordance with reports in the literature for Ru^{II} complexes with phosphine and diimine ligands.[31,32]

The details of the X-ray structure obtained for the new complex are explained in the Experimental section and the structural data are given in Table 1. The molecular structure of the complex is displayed as an ORTEP representation in Figure 5, and selected bond distances and angles are shown in Table 2.

Observing the crystallographic data, it can be confirmed that in the coordination sphere of the complex there are two bidentate ligands (44bipy and dppb), a chlorido ligand and a 4-pic ligand, and the PF_6^- is the counter ion. The complex crystallizes in a monoclinic $P2_1/n$ centrosymmetric group, with one molecule *per* asymmetric unit and the structure is in accordance with the NMR, IR and cyclic voltammetry results.

The compound has distorted octahedral geometry, with a large deviation from the ideal angle of 90°, where P(1)–Ru–P(2) is 93.44°, N(1)–Ru–N(2) is 77.84° and Cl–Ru–N4pic is 87.11°, which are very close to values shown for similar complexes. The Ru–N4pic bond lengths are 2.330 Å, Ru–P(1) is 2.342 Å and the bond length of

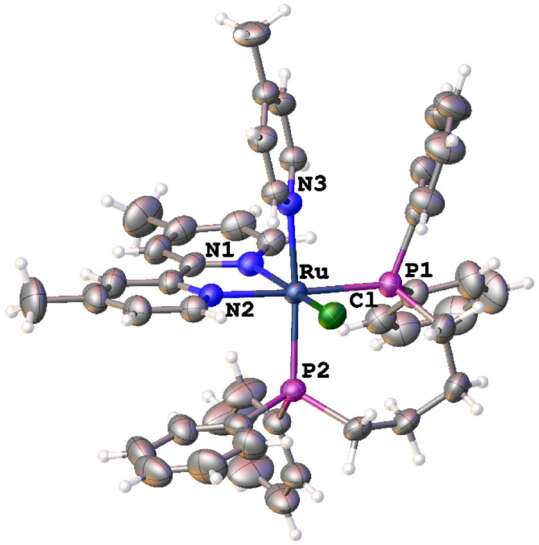

Figure 5. ORTEP view of RuCl(dppb)(44bipy)(4-pic)]PF_6 complex with thermal ellipsoids are drawn at a 50% probability limit. The PF_6^- counterion was omitted for clarity.

Table 1. Crystal data and structure refinement for [RuCl(dppb)(44bipy)(4-pic)]PF_6

Identification code	C4B-4pic
Empirical formula	$C_{46}H_{47}ClF_6N_3P_3Ru$
Formula weight / (g mol^{-1})	985.29
Temperature / K	296.15
Crystal system	monoclinic
Space group	$P2_1/n$
a / Å	13.1542(4)
b / Å	16.6476(5)
c / Å	22.7227(7)
α / degree	90
β / degree	100.2120(10)
γ / degree	90
Volume / $Å^3$	4897.1(3)
Z	4
ρ_{calc} / (g cm^{-3})	1.336
μ / mm^1	0.529
F(000)	2016.0
Crystal size / mm^3	0.28 × 0.22 × 0.18
Radiation	Mo Kα (λ = 0.71073)
2θ range for data collection / degree	3.05 to 51.996
Index ranges	−15 ≤ h ≤ 16, −20 ≤ k ≤ 20, −27 ≤ l ≤ 27
Reflections collected	142172
Independent reflections	9629 [R_{int} = 0.0565, R_{sigma} = 0.0233]
Data/restraints/parameters	9629/0/544
Goodness-of-fit on F^2	1.042
Final R indexes (I > = 2σ(I))	R_1 = 0.0414, wR_2 = 0.1040
Final R indexes (all data)	R_1 = 0.0473, wR_2 = 0.1078
Largest diff. peak/hole / (e $Å^{-3}$)	0.89/−0.51

a-c and α-γ: unit cell parameters; Z: formula unit *per* unit cell; F(000): structure factor in the zeroth-order case; F^2: squared structure factor; R_1 and wR_2: R-factor and weighted R-factor, respectively.

Table 2. Optimized and experimental geometries bond lengths and angles for complex [RuCl(dppb)(44bipy)(4-pic)]PF_6

	Experimental	Calculated
	Bond / Å	
Ru1–N4pic	2.194(2)	2.255
Ru1–P1	2.342(1)	2.482
Ru1–P2	2.330(8)	2.430
Ru1–N1	2.081(3)	2.121
Ru1–N2	2.116(3)	2.128
Ru1–Cl	2.421(9)	2.495
	Angle / degree	
$N_{4\text{-pic}}$–Ru1–Cl	88.25(7)	89.56
N1–Ru1–N2	77.80(1)	77.08
P1–Ru–P2	93.45(3)	97.72

the P *trans* to the 4pic ligand, Ru–P(2), is slightly lower with 2.330 Å.[8,13,16,21]

The selected bond lengths are shown in Table 2 and are in accordance with the data available in the Cambridge Crystallographic Data Centre (CCDC) database when the data are compared with bond lengths and angles for all similar structures available in the Crystal Structure Database (CSD) using the Mogul software.[33]

Computational analysis

It is already well established in the literature that ruthenium(II) compounds are low spin diamagnetic, and therefore have the electronic state $(dxy)^2(dxz)^2(dyz)^2(dz_2)^0(dx_2\text{-}y_2)^0$ in the ground state. This means that the structure was optimized in the singlet state by the analysis of the absence of imaginary frequencies.[34]

The optimized structure of the complex [RuCl(dppb)(44bipy)(4-pic)]$^+$ at the DFT/B3LYP level was superimposed with the data obtained experimentally for the sake of comparison, as shown in Figure 6.

The selected bond lengths and angles are shown in Table 2, which corresponds to the optimized geometrical parameters of the compound at the DFT/B3LYP level and the experimental data. It can be observed that the optimized structure is in accordance with the crystallographic data obtained, as already reported in the literature where the B3LYP functional presented accurate results to predict geometric parameters, which are very close to the experimental data.[35-39]

It is of the utmost importance to know the physico-chemical parameters of the system and its energy from the frontier orbitals (highest occupied molecular orbital (HOMO) and the lowest unoccupied molecular orbital (LUMO)) that provides valuable quantum information. Thus, the energy of the frontier orbitals were calculated

Figure 6. Overlap of structures obtained experimentally (red) and optimized by DFT (yellow) for the $[RuCl(dppb)(44bipy)(4\text{-}pic)]^+$ complex.

(E_{HOMO} and E_{LUMO}) and the HOMO-LUMO gap for the $[RuCl(dppb)(44bipy)(4\text{-}pic)]^+$ complex in vacuum are presented in Figure 7.[40,41] The HOMO orbital is centered mainly on the d(Ru) and p_x orbitals of the Cl atom, and the LUMO orbital is centered on the 44bipy diiminic ligand. The calculated gap for the HOMO and LUMO orbitals was 3.1062 eV.

TD-DFT calculations were performed in order to predict UV-Vis spectrum for the first 80 excitations and the results

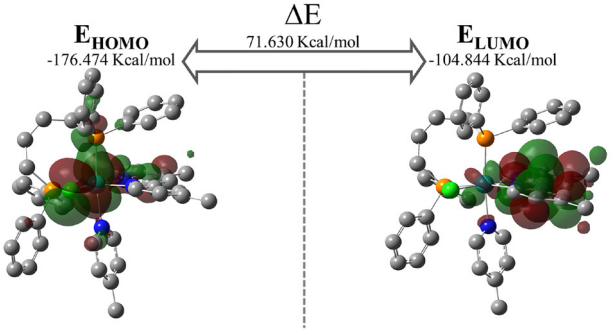

Figure 7. Representation of HOMO and LUMO orbitals obtained for the $[RuCl(dppb)(44bipy)(4\text{-}pic)]^+$ complex in vacuum.

were compared with the experimentally obtained UV-Vis spectrum. Theoretically and experimentally obtained UV spectra are in good agreement and both indicate two main absorption peaks, which are summarized (excitation energies, wavelength and oscillator strengths) in Table 3. The difference of the wavelengths between theoretically and experimentally obtained UV spectra is around 10 nm, which is in good agreement. (Figure S10, SI section).

The band located at 290 nm in the experimental spectrum appears at 280 nm in the theoretical spectrum is due to a transition of the type π-π*, which has the greatest contribution of the HOMO-11 → LUMO transition (34.1%). The second band of the experimental spectrum is at 438 nm, which is correspondent to the peak located at 450 nm in the theoretical spectrum. This transition is of the metal-to-ligand charge-transfer (MLCT) type since the transition is from the Ru-centered orbitals (dπ), the π* type orbitals of the Cl ligand and bipyridine ligands. This transition is mainly formed by the HOMO-2 → LUMO orbitals with 88.0% of contribution and HOMO → LUMO 4.4% of contribution. All the theoretical data showed good agreement with the experimental data, which corroborates the theoretical model used.

Catalytic transfer hydrogenation reaction

The $[RuCl(dppb)(44bipy)(4\text{-}pic)]PF_6$ complex was evaluated as a catalyst precursor with hydrogen transfer reaction activity from isopropanol (2-propanol) to ketones (Figure 8). The C4B-4pic was evaluated in air using isopropanol as a hydrogen source and different ketone substrates (acetophenone, cyclohexanone and methyl-ethyl-ketone).

NMR techniques are widely used to detect multiple reactive intermediates, providing thereby important information concerning the involved reaction mechanism.[15] The Figure 9 allows to follow the catalytic reaction with the expansion of the ^1H NMR spectra, the hydrogen transfer reaction using isopropanol as a hydrogen donor, precatalyst $[RuCl(dppb)(44bipy)(4\text{-}pic)]PF_6$ complex,

Table 3. The λ_{max} (experimental) and λ_{max} (calculated), energy, oscillator strengths (f), selected transitions (orbitals and contribution) and type of electronic transition of the $[RuCl(dppb)(44bipy)(4\text{-}pic)]PF_6$

λ_{max} exp. / nm	λ_{max} cal. / nm	Energy / eV	f	Transitions	Character
290	280	4.4642	0.1165	HOMO-11 → LUMO (34.1%) HOMO → LUMO +7 (19.2%) HOMO-12 → LUMO+1 (14.4%)	π-π*
438	450	2.7474	0.0431	HOMO-2 → LUMO (88.0%) HOMO → LUMO (4.4%) HOMO → LUMO+5 (1.1%)	MLCT

HOMO: highest occupied molecular orbital; LUMO: the lowest unoccupied molecular orbital; MLCT: metal-to-ligand charge-transfer.

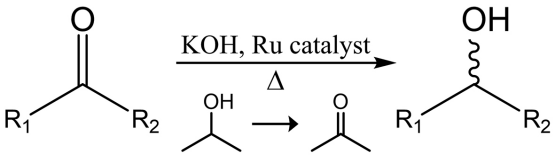

Figure 8. Proposed hydrogen transfer reaction based on Ru^{II} transfer of isopropanol ketones.

and acetophenone as substrate. Beforehand, the reaction monitored by NMR spectroscopy from 6.8 to 7.8 ppm, showed the three acetophenone signals, at 7.77, 7.36, and 7.26 ppm. During the reaction, these three peaks decreased with a concomitant increase of three peaks at 7.23, 7.12, and 7.02 ppm, which can be attributed to the reduced product, acetophenol. During the reaction, the formation of the acetone singlet at 1.9 ppm and the acetophenol doublet at 1.32 ppm were observed. The spectra in Figure 9 demonstrate the continuous formation of the products during a 6 h reaction. The transfer hydrogenation reaction was also performed using hexanone and methyl ethyl ketone as substrate and monitored with NMR.

The data presented in Table 4 show the efficiency of the C4B-4pic complex in the hydrogenation transfer reaction at 60 ºC. The pre-catalyst shows efficient conversion of the product, always higher than 80%. In articles previously published in the literature,[15,42] it is common to use nitrogen atmosphere, in addition to high temperature (82 ºC) and a catalyst load between 0.1 to 1 mol%. A recent study[15] used temperatures of 40 and 50 ºC, a catalyst load of 5% and a reaction time between 24 to 30 h.

These observations reinforce that the use of an inert atmosphere was needless, with an acceptable reaction time. The catalyst load is similar and the *in situ* conditions were performed in the NMR equipment. It is worth mentioning that the reaction itself occurs only in the presence of the pre-catalyst and the base.

Table 4. Performance of the Ru^{II} complex in the transfer hydrogenation of ketones

entry	Substrate[a]	Conversion[b] / %	TON[c]	TOF[d]
1	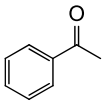	81	162	27
2	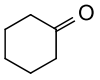	98	196	33
3	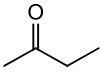	87	174	29

[a]Reactions were carried out at 60 °C during 6 h, using isopropanol (520 µL), ketone (0.5 mmol), base (10 mol%) and catalyst (0.5 mol%); [b]conversion was monitored by ^{1}H NMR spectroscopy using C_6D_6 as the solvent and internal standard; [c]TON: turnover number: ratio of formed product moles to consumed catalyst moles; [d]TOF: TON/time (h^{-1}).

A widely accepted mechanism for catalytic activity of ruthenium complexes in the base-assisted transfer hydrogenation from isopropanol to ketones involves the dissociation of the chlorido ligand, as well as the coordination of the hydride species. A plausible mechanism for the catalytic activity of the Ru^{II} complex used here is presented in Figure 10.

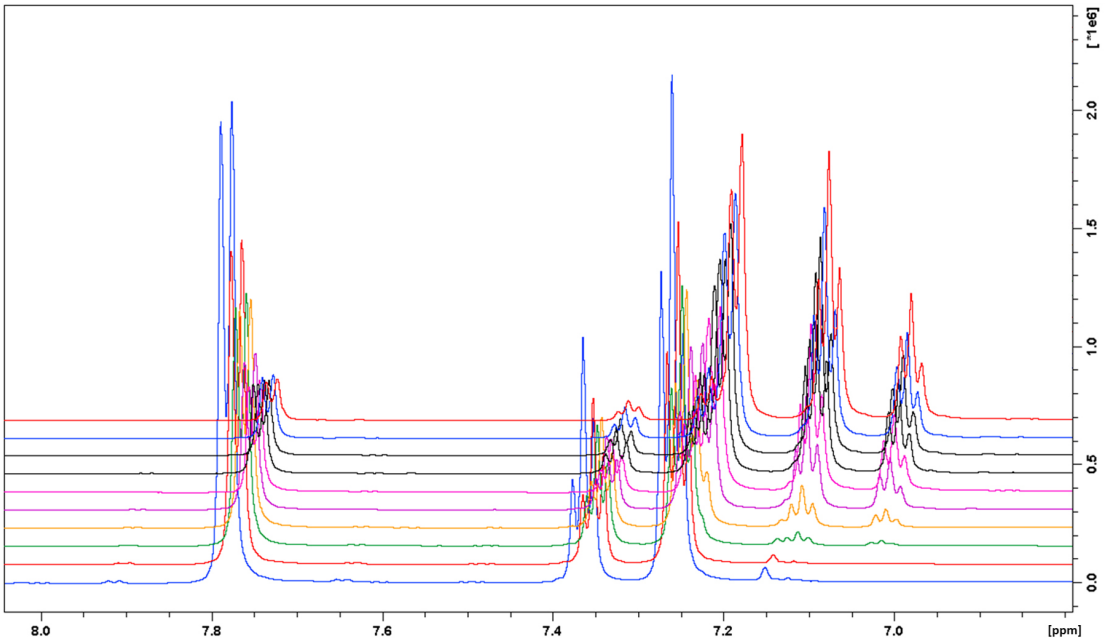

Figure 9. Selected ^{1}H NMR spectra (6.5-8.0 ppm) obtained by monitoring the hydrogen transfer reaction in acetophenone at 50 s intervals for 6 h. For clarity, the figure shows only the selected experiments obtained every 2150 s.

It was previously proposed by Aydemir *et al.*[43] that the first step comprised the removal of the isopropanol more acidic hydrogen by the base, as well as the formation of ions that react with the pre-catalyst A, forming the Ru-iso-propoxyde species B. The B intermediate undergoes β-hydride elimination and forms the ruthenium species C, D and acetone. Then, the hydride intermediates C and D react with the carbonyl carbons of ketones substrate and lead to the alkoxyde substrates E and F. Finally, the alkoxide substrates react with another isopropanol molecule (in excess), restoring the intermediate B by releasing the respective alcohol derived from the substrate.

In order to corroborate the proposed mechanism, NMR spectra of solutions containing isopropanol, base and the pre-catalyst A were acquired, as shown in Figure 11. The insets in the spectra evidence two groups of signals, one doublet of doublets (dd) around −14.0 ppm, and one triplet (t) at approximately −14.4 ppm. Weak signals were attributed to the coupling between hydrogen and phosphorous atoms of the hydride intermediates, which

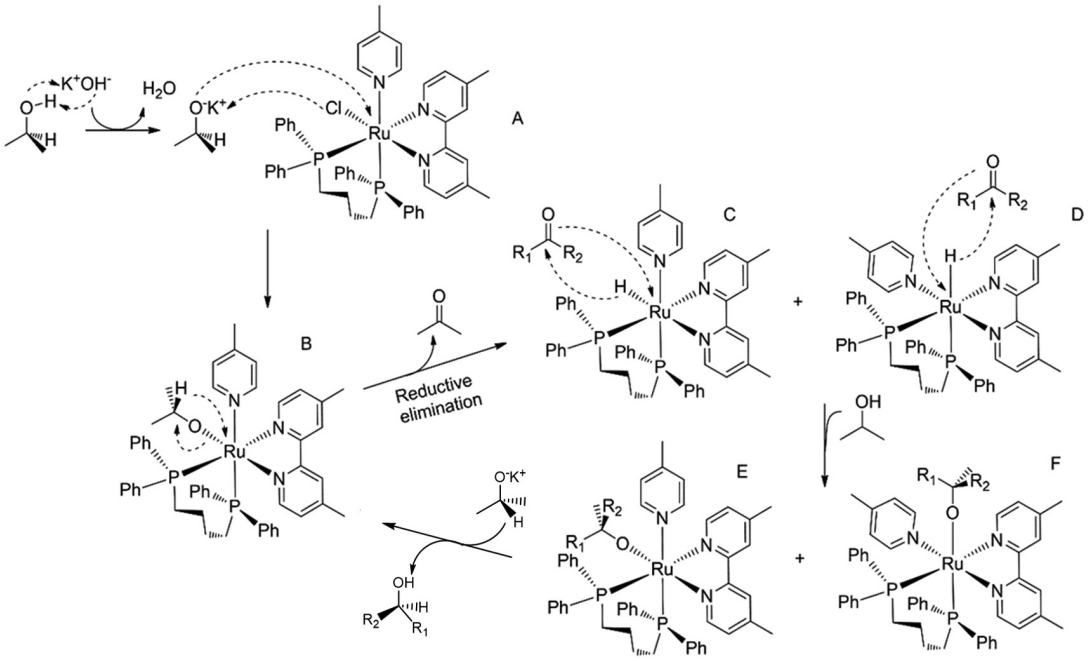

Figure 10. Proposed mechanism for the transfer hydrogenation of ketones catalyzed by the [RuCl(dppb)(44bipy)(4-pic)]PF_6 complex.

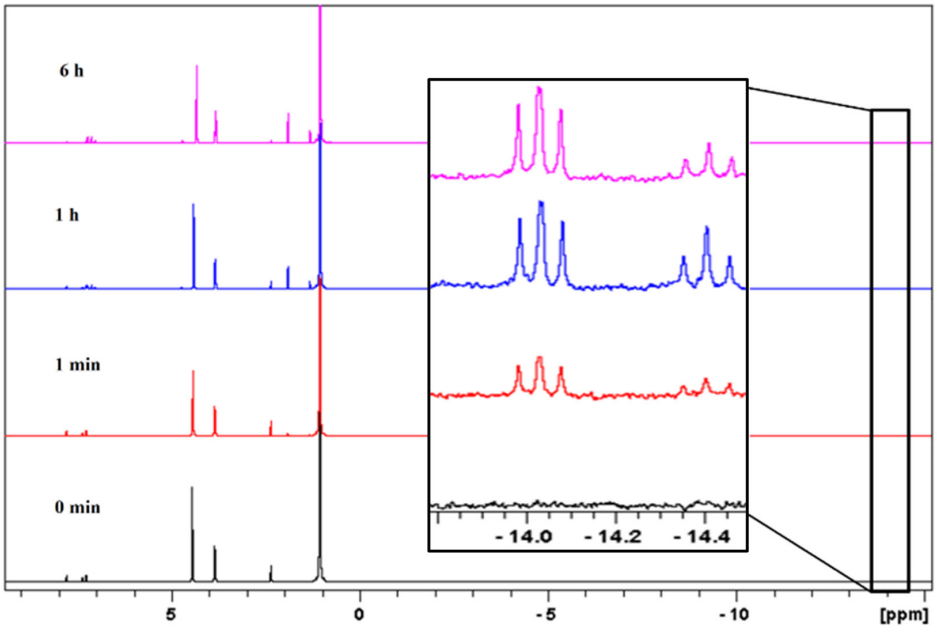

Figure 11. ^{1}H NMR spectra (400.21 MHz, C_6D_6) showing the formation of hydride signals for [RuCl(dppb)(44bipy)(4-pic)]PF_6 complex.

occurs at a low concentration (0.1%). The dd signal is originated by the coupling with one phosphorus-*trans* and one phosphorus atom in the *cis* position. The t signal is attributed to the coupling of the hydride with two phosphorus atoms in the *cis* position.

The ^{1}H NMR experiments allowed to observe the formation of two species of ruthenium hydride in the initial stage of the hydrogen transfer reaction.[42] The hydride generated can be observed until the end of the reaction.

Conclusions

We have described the synthesis of a mononuclear ruthenium(II) complex, which presents an octahedral geometry around the metal center, containing two bidentate ligands (phosphine and diimine) and two monodentate ligands (chlorido and 4-picoline) suggested by FTIR and ^{31}P{^{1}H}, ^{1}H and ^{13}C{^{1}H} NMR spectroscopy, where the ligand 4-picoline is *trans* to the phosphorous atom of the phosphine ligand. This structure was confirmed by single crystal X-ray diffraction. The calculations by DFT methods at the B3LYP/Lanl2dz/6-31G* level of theory are in agreement with experimental structural parameters. In the frontier molecular orbitals, the HOMO is centered mainly on the d(Ru) orbitals and the p_x orbitals of the Cl atom, while the LUMO is centered mainly on the 44bipy diiminic ligand. The HOMO-LUMO gap was calculated at 3.1062 eV. Analysis of the UV-Vis spectrum of the complex showed good agreement of the experimental and the calculated data, which showed a difference of only 10 nm for the two main absorptions peaks. The study of the catalytic activity in the transfer hydrogenation of ketones by the ^{1}H NMR technique showed that the complex is efficient on the transfer hydrogenation reaction at 60 ºC and uses acetophenone as substrate with good conversion, where two ruthenium-hydride species are formed at the initial stage of the hydrogen transfer reaction during 6 h. The yield of the hydrogenation process was higher than 80% in the concentration studied, and the results obtained are as good as those presented in the literature showing that the complex could be used as a catalyst for the transfer hydrogenation reaction of acetophenone.

Supplementary Information

Crystallographic data for the structure [RuCl(dppb)(44bipy)(4-pic)]PF_6 reported in this paper have been deposited with the Cambridge Crystallographic Data Center, CCDC No. 1893634. Copies of the data can be obtained free of charge on application to CCDC, 12 Union Road, Cambridge CB2 1EZ, UK (fax: +44 1223 336033; e-mail: deposit@ccdc.cam.ac.uk or http://www.ccdc.cam.ac.uk).

The data of all NMR experiments as well as potential energy distribution analysis and some theoretical results, geometric and electronic parameters are available free of charge at http://jbcs.sbq.org.br as PDF file.

Acknowledgments

This study was financed in part by the Coordenação de Aperfeiçoamento de Pessoal de Nível Superior Brazil (CAPES) - Finance Code 001, CNPq, CENAPAD and FAPESP.

Author Contributions

Rafael G. Silveira was responsible for conceptualization, investigation, formal analysis and writing original draft and editing; Angel R. Higuera-Padilla for investigation, formal analysis and writing original draft and editing; Beatriz N. da Cunha for investigation, formal analysis and writing original draft and editing; João Honorato for investigation, formal analysis and writing original draft and editing; Luiz A. Colnago for formal analysis and resources; Anderson Catão for formal analysis and writing original draft and editing; Eduardo E. Castellano for formal analysis and resources; Alzir A. Batista for conceptualization, writing original draft and editing, funding acquisition, project administration and resources.

References

1. Pagliaro, M.; Campestrini, S.; Ciriminna, R.; *Chem. Soc. Rev.* **2005**, *34*, 837.
2. Naota, T.; Takaya, H.; Murahashi, S. I.; *Chem. Rev.* **1998**, *98*, 2599.
3. Johansson, J. R.; Beke-Somfai, T.; Said Stålsmeden, A.; Kann, N.; *Chem. Rev.* **2016**, *116*, 14726.
4. Zhou, Y. B.; Tang, F. Y.; Xu, H. D.; Wu, X. Y.; Ma, J. A.; Zhou, Q. L.; *Tetrahedron: Asymmetry* **2002**, *13*, 469.
5. Sanchez-Delgado, R. A.; Bradley, J. S.; Wilkinson, G.; *Dalton Trans.* **1976**, *1*, 399.
6. Bień, M.; Pruchnik, F. P.; Seniuk, A.; Lachowicz, T. M.; Jakimowicz, P.; *J. Inorg. Biochem.* **1999**, *73*, 49.
7. da Silva, J. P.; Silva, I. C.; Pavan, F. R.; Back, D. F.; de Araujo, M. P.; *J. Inorg. Biochem.* **2017**, *173*, 134.
8. Honorato, J.; Oliveira, K. M.; Leite, C. M.; Colina-Vegas, L.; Nóbrega, J. A.; Castellano, E. E.; Ellena, J.; Correa, R. S.; Batista, A. A.; *J. Braz. Chem. Soc.* **2020**, *31*, 2237.
9. Landaeta, V. R.; la Rosa, A. D. S.; Rodríguez-Lugo, R. E.; *Inorg. Chim. Acta* **2018**, *470*, 303.

10. Ruff, A.; Kirby, C.; Chan, B. C.; O'Connor, A. R.; *Organometallics* **2016**, *35*, 327.
11. Ikariya, T.; Blacker, A. J.; *Acc. Chem. Res.* **2007**, *40*, 1300.
12. Fujii, A.; Hashiguchi, S.; Uematsu, N.; Ikariya, T.; Noyori, R.; *J. Am. Chem. Soc.* **1996**, *118*, 2521.
13. Ribeiro, M. C.; Corrêa, R. S.; Barbosa, M. I. F.; Delolo, F. G.; Ellena, J.; Bogado, A. L.; Batista, A. A.; *Polyhedron* **2017**, *137*, 311.
14. Rodrigues, C.; Delolo, F. G.; Norinder, J.; Börner, A.; Bogado, A. L.; Batista, A. A.; *J. Mol. Catal. A: Chem.* **2017**, *426*, 586.
15. Higuera-Padilla, A. R.; Batista, A. A.; Colina-Vegas, L.; Villarreal, W.; Colnago, L. A.; *J. Coord. Chem.* **2017**, *70*, 3541.
16. Queiroz, S. L.; Batista, A. A.; Oliva, G.; Gambardella, M. T. P.; Santos, R. H. A.; MacFarlane, K. S.; Rettig, S. J.; James, B. R.; *Inorg. Chim. Acta* **1998**, *267*, 209.
17. Sheldrick, G. M.; *Acta Crystallogr., Sect. A: Found. Adv.* **2015**, *A71*, 3.
18. Dolomanov, O. V.; Bourhis, L. J.; Gildea, R. J.; Howard, J. A. K.; Puschmann, H.; *J. Appl. Crystallogr.* **2009**, *42*, 339.
19. Macrae, C. F.; Bruno, I. J.; Chisholm, J. A.; Edgington, P. R.; McCabe, P.; Pidcock, E.; Rodriguez-Monge, L.; Taylor, R.; van de Streek, J.; Wood, P. A.; *J. Appl. Crystallogr.* **2008**, *41*, 466.
20. Frisch, M. J.; Trucks, G. W.; Schlegel, H. B.; Scuseria, G. E.; Robb, M. A.; Cheeseman, J. R.; Scalmani, G.; Barone, V.; Mennucci, B.; Petersson, G. A.; Nakatsuji, H.; Caricato, M.; Li, X.; Hratchian, H. P.; Izmaylov, A. F.; Bloino, J.; Zheng, G.; Sonnenberg, J. L.; Hada, M.; Ehara, M.; Toyota, K.; Fukuda, R.; Hasegawa, J.; Ishida, M.; Nakajima, T.; Honda, Y.; Kitao, O.; Nakai, H.; Vreven, T.; Montgomery Jr., J. A.; Peralta, J. E.; Ogliaro, F.; Bearpark, M. J.; Heyd, J.; Brothers, E. N.; Kudin, K. N.; Staroverov, V. N.; Kobayashi, R.; Normand, J.; Raghavachari, K.; Rendell, A. P.; Burant, J. C.; Iyengar, S. S.; Tomasi, J.; Klene, M.; Knox, J. E.; Cross, J. B.; Bakken, V.; Adamo, C.; Jaramillo, J.; Gomperts, R.; Stratmann, R. E.; Yazyev, O.; Austin, A. J.; Cammi, R.; Pomelli, C.; Ochterski, J. W.; Martin, R. L.; Morokuma, K.; Zakrzewski, V. G.; Voth, G. A.; Salvador, P.; Dannenberg, J. J.; Dapprich, S.; Daniels, A. D.; Farkas, Ö.; Foresman, J. B.; Ortiz, J. V.; Cioslowski, J.; Fox, D. J.; Cossi, M.; Rega, N.; Millam, N.; *Gaussian 09*, version E.01; Gaussian, Inc.: Wallingford, CT, USA, 2009.
21. Barbosa, M. I. F.; Correa, R. S.; Bastos, T. M.; Pozzi, L. V.; Moreira, D. R. M.; Ellena, J.; Doriguetto, A. C.; Silveira, R. G.; Oliveira, C. R.; Kuznetsov, A. E.; Malta, V. S.; Soares, M. B. P.; Batista, A. A.; *New J. Chem.* **2017**, *41*, 4468.
22. Lima, B. A. V.; Corrêa, R. S.; Graminha, A. E.; Varela Jr., J. J. G.; da Silva, A. B. F.; Ellena, J.; Silva, T. E. M.; Batista, A. A.; *J. Braz. Chem. Soc.* **2020**, *31*, 1352.
23. Adeniyi, A. A.; Ajibade, P. A.; *Spectrochim. Acta, Part A* **2013**, *115*, 426.
24. Kang, R.; Yao, J.; Chen, H.; *J. Chem. Theory Comput.* **2013**, *9*, 1872.
25. Monteiro, M. C. R.; Nascimento, F. B.; Valle, E. M. A.; Ellena, J.; Castellano, E. E.; Batista, A. A.; Machado, S. P.; *J. Braz. Chem. Soc.* **2010**, *21*, 1992.
26. Silveira, R. G.; Catão, A. J. L.; Cunha, B. N.; Almeida, F.; Correa, R. S.; Diniz, L. F.; Tenório, J. C.; Ellena, J.; Kuznetsov, A. E.; Batista, A. A.; Alcântara, E.; *J. Braz. Chem. Soc.* **2018**, *29*, 2502.
27. Wang, T.-H.; Hsiao, C.-H.; Chen, S.-H.; Cheng, Y.-T.; Chen, L.-Y.; *Polyhedron* **2015**, *102*, 216.
28. Leonid, S.; *Chemissian: Software to Analyze Spectra, Build Density Maps and Molecular Orbitals*, version 4.53; Chemissian, Inc.: Saint Petersburg, Russia, 2016.
29. McGarrity, J. F.; Prodolliet, J.; *J. Org. Chem.* **1984**, *49*, 4465.
30. McGarrity, J. F.; Prodolliet, J.; Smyth, T.; *J. Magn. Reson.* **1981**, *17*, 59.
31. Chandra, S.; Kumar, R.; *Spectrochim. Acta, Part A* **2005**, *62*, 1050.
32. Correa, R. S.; da Silva, M. M.; Graminha, A. E.; Meira, C. S.; Santos, J. A.; Moreira, D. R.; Soares, M. B.; Von Poelhsitz, G.; Castellano, E. E.; Bloch Jr., C.; Cominetti, M. R.; Batista, A. A.; *J Inorg. Biochem.* **2016**, *156*, 153.
33. Bruno, I. J.; Cole, J. C.; Kessler, M.; Luo, J.; Motherwell, W. D. S.; Purkis, L. H.; Smith, B. R.; Taylor, R.; Cooper, R. I.; Harris, S. E.; Orpen, A. G.; *J. Chem. Inf. Comput. Sci.* **2004**, *44*, 2133.
34. Tavakol, H.; *Arabian J. Chem.* **2017**, *10*, S786.
35. Mohamed, R. G.; Elantabli, F. M.; Abdel Aziz, A. A.; Moustafa, H.; El-Medani, S. M.; *J. Mol. Struct.* **2019**, *1176*, 501.
36. Gloriozov, I. P.; Nechaev, M. S.; Zaitsev, K. V.; Oprunenko, Y. F.; Gam, F.; Saillard, J. Y.; *J. Organomet. Chem.* **2019**, *889*, 9.
37. Tsipis, A. C.; *Coord. Chem. Rev.* **2014**, *272*, 1.
38. Kamalesu, S.; Swarnalatha, K.; Subramanian, R.; Muralidharan, K.; Gomathi, S.; *Inorg. Chim. Acta* **2017**, *461*, 35.
39. Alperovich, I.; Moonshiram, D.; Concepcion, J. J.; Pushkar, Y.; *J. Phys. Chem. C* **2013**, *117*, 18994.
40. Fukui, K.; *Science* **1982**, *218*, 747.
41. Gómez-Jeria, J. S.; *J. Chil. Chem. Soc.* **2010**, *55*, 381.
42. Schott, D.; Sleigh, C. J.; Lowe, J. P.; Duckett, S. B.; Mawby, R. J.; Partridge, M. G.; *Inorg. Chem.* **2002**, *41*, 2960.
43. Aydemir, M.; Meric, N.; Baysal, A.; Turgut, Y.; Kayan, C.; Şeker, S.; Toğrul, M.; Gümgüm, B.; *J. Organomet. Chem.* **2011**, *696*, 1541.

Submitted: February 6, 2021
Published online: May 12, 2021